Compactification of a Myelin Mimetic Langmuir Monolayer upon Adsorption and Unfolding of Myelin Basic Protein

Z. Khattari,[†] Y. Ruschel,[‡] H. Z. Wen,[§] A. Fischer,[⊥] and T. M. Fischer*[,§]

Institut für Röntgenphysik, Universität Göttingen, 37073 Göttingen, Germany, Institut für Chemie, Universität Potsdam, 14476 Golm, Germany, Department of Chemistry and Biochemistry, The Florida State University, Tallahassee, Florida 32306-4390, and Max Planck Institute of Colloids and Interfaces, 14424 Potsdam, Germany

Received: October 4, 2004

The surface shear viscosity of a myelin mimetic Langmuir monolayer is investigated upon adsorption of myelin basic protein (MBP). We measure an increase of the surface shear viscosity at picomolar concentrations of the protein, suggesting that the globular conformation of MBP changes upon adsorption at the monolayer. The conformational change enables hydrodynamic interactions of the proteins, with a typical separation of hundreds of nanometers. This unfolding is essential for the compactification of the myelin sheath, serving an enhanced saltatory signal transduction in vertebrates. The viscometry used extends the sensitivity of standard surface viscometers toward lower viscosities.

Introduction

Myelin is generated by oligodendrocytes in the central and by Schwann cells in the peripheric nervous system. It is a membrane structure necessary for the isolation of special nervous fibers enabeling a fast saltatory signal transduction[1] therein and contains around 30% protein. One part of that is the myelin basic protein (MBP), a highly basic protein with isoelectric points greater than 10.[2] By alternative splicing, different highly variations of the basic protein (14−21 kDa) could be isolated (see ref 3 for a review). Corresponding to the surrounding conditions, the numerous hydrophobic side chains of the polypeptide main chain fold spontaneously to the molecule inside to the molecule surface. Because of this, MBP generates a random coil formation[4−6] when dissolved in water and an α-helical or β-sheet structure[7−9] when interacting predominantly electrostatically with acidic lipids[10−16] of the membrane. One of the functions of MBP is to compactify the polylayer,[17] which forms the myeline sheath of nervous cells of vertebrates. MBP also plays a key role in the process of demyelination—the destruction, loss, or removal of the myelin sheath—and is involved in the chronic desease of multiple sclerosis that results in demyelination, following damage to axons, myeline, oligodendrocytes, or neurons. Mutants of the protein are used to induce allergic encephalomyelitis.

Compaction results in a specific increase of the surface shear viscosity of a fluid membrane, i.e., a decrease in mobility of membrane bound objects upon adsorption of MBP. Different techniques are used to measure the mobility of membrane bound objects. Fluorescence probes,[18,19] NMR,[20,21] and particle tracking techniques[22] are employed to study the lateral and rotational mobility of proteins or membrane bound structures to gain insight into immunological, hormonal, and signal transduction reactions. Saffman and Delbrück[23] and Hughes, Pailthorpe, and White[24] derived the fundamental relations between the translational and rotational mobilities and the collective mechanic bulk and membrane parameters, i.e., the surface shear viscosity η_s of the membrane and the bulk shear viscosity η of the adjacent phases. The relations are used experimentally to infer hydrodynamic radii of membrane bound structures[25] below the microscopic resolution. On the microscopic scale, optical tweezers are used to obtain coarse-grained surface shear viscosities[26] of Langmuir monolayers, which often mimic the essentials of one leaflet of biological membranes.

Materials and Methods

Lipid-free MBP, sodium dodecyl sulfate (SDS), and methyl octadecanoate are purchased from Sigma. MBP is extracted from bovine central nervous system and is claimed to be 99+% pure. Silica beads (diameter 3−10 μm, Bangs Laboratories) are rinsed in a HCl/chloroform mixture and then immersed into pure chloroform. Octadecanoate and silica beads are both spread from chloroform (Merck) onto the air/water interface. Without further purification MBP (SDS) has been dissolved in deionized water (Millipore Milli-Q, 18 MΩ) at concentrations of the order (0.5 μM). In the fluorescence microscopy experiments it is added close to the objective to the subphase consisting of deionized water (Millipore Milli-Q, 18 MΩ) using a syringe. After that, the Langmuir trough was left for equilibration of the protein for 1 h. Subphase concentrations are calculated under the assumption of a homogeneous equilibration in the entire subphase.

A schematic drawing of the combination of tweezers with fluorescence microscopy is shown in Figure 1. Two simultaneous operations are performed by a 100× water immersion objective, numerical aperture 1.0, built into the bottom of a temperature-controlled film balance. First, it projects a fluorescence image of the monolayer onto a SIT camera (Hamamatsu C 3077-01). Fluorescence is excited in the labeled (1% 4-hexadecylamino-7-nitrobenz-2-oxa-1,3-diazole, Molecular Probes) monolayer by a p-polarized argon ion laser (488 nm, 150 mW). The excitation light is blocked by a filter in front of

[†] Universität Göttingen.
[‡] Universität Potsdam.
[§] The Florida State University.
[⊥] Max Planck Institute of Colloids and Interfaces.
* Corresponding author: e-mail tfischer@chem.fsu.edu.

10.1021/jp045493z CCC: $30.25
Published on Web 02/01/2005

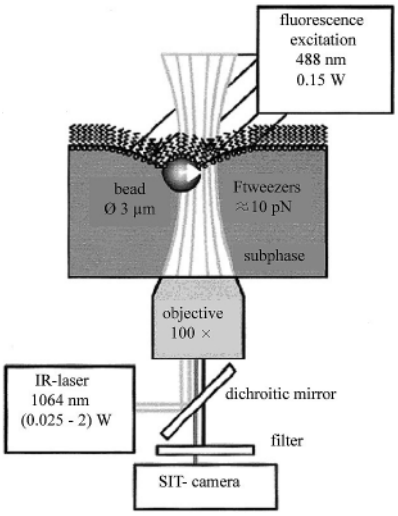

Figure 1. Scheme of the setup combining fluorescence microscopy with optical tweezers.

the detector. Second, two IR laser beams ($\lambda = 1064$ nm, $P =$ 10 mW−2 W), coupled into the optical path using a dichroic mirror (transparent for fluorescence light), are focused by the objective onto the monolayer. The diameter of the beams is fit to the objective entrance in order to maximize the lateral optical forces. Before the beams are reflected at the dichroic mirror, both are focused separately using Galilei optics at the air−water interface, where one of the beams can be moved laterally by two rotating mirrors (not shown in Figure 1). The absorption of the laser in the water causes an increase in temperature at the focus proportional to the laser power of the order of 10 K/W. The fluorescence dye in the monolayer when being illuminated by either the weakly focused Ar^+ laser or the strongly focused IR laser is no significant heat source. We operated both lasers at a power around 150 mW.

The experiments are performed in the coexistence region liquid condensed (LC)/liquid expanded (LE) at a temperature of $\vartheta = 35$ °C. Silica beads [Bangs Laboratories, diameter = 4.8 μm] are immersed into the monolayer by spreading from a chloroform suspension. They absorb at the LC/LE boundaries via dipole−dipole interaction.[27] In Figure 2 the capture ($t = 0$ s) and consecutive motion of a LC domain (radius $a = 30$ μm) around the tweezers is shown. An adsorbed bead, captured by the tweezers, fixes a specific point of the domain boundary. Air convection above the monolayer causes a homogeneously flow at constant velocity ($U = 80$ μm/s) from the lower left to the upper right of the image. The domain rotates around the tweezers position until the flow direction and the orientation of the domain are aligned ($t = 0-1.2$ s). If we are working at higher dye concentration, the actual orientation of the domain can be inferred from the internal anisotropic texture. No slip of the bead at the boundary is observed under these conditions. Upon reaching the equilibrium position, the domain starts to deform ($t = 0.4-1.2$ s).[28] We infer the monolayer viscosity from this experiment by solving the hydrodynamics of a solid disk of radius a being immersed into a homogeneous infinitely extended monolayer of surface shear viscosity η_s on top of a infinitely deep subphase of viscosity η. Under the influence of an external force attached to the perimeter, the domain starts a combined translational and rotational motion in a continuosly translating monolayer environment of velocity U, which aligns the domain with the flow direction (Figure 2). Under the above assumptions the angle $\varphi(t)$ between the domain and the flow

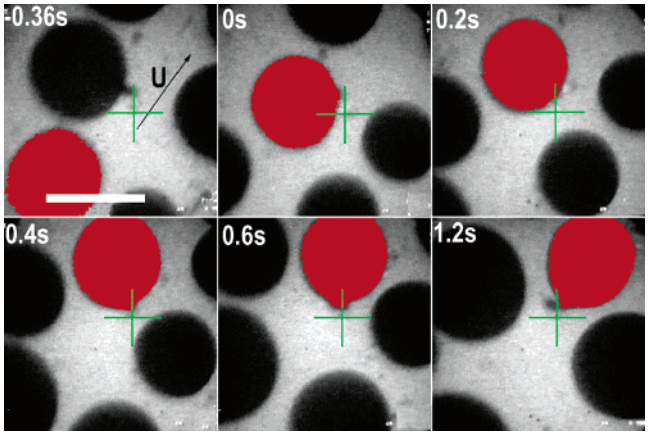

Figure 2. Consecutive fluorescence microscopy images of a liquid condensed domain (colored red), with a silica bead attached to it (nonfluorecent) in coexistence with a liquid expanded phase (bright) on a $c = 1.1$ nmol/L myelin basic protein containing subphase. At $t =$ 0 s the bead is trapped in the tweezers (cross hair) and aligning with the flow ($t = 0-1.2$ s) of the liquid expanded. Adsorbing myelin basic protein increases the surface shear viscosity of the liquid expanded phase and slows down the alignment. The bar is 60 μm.

direction is related to the distance $x = Ut$ a noncaptured domain moves in the same time:[29]

$$\ln \tan(\varphi/2) = -\frac{1}{1 + f_R/f_T}\frac{Ut}{a} \tag{1}$$

where a is the radius of the rotating bead and $f_R(B)$ and $f_T(B)$ are dimensionless rotational and translational friction coefficients[24] (Appendix):

$$\frac{f_R}{f_T} = \begin{cases} \frac{2}{3}\left(1 + \left[\frac{6}{\pi} - 1\right]B\right) + O(B^2) & \text{for } B \ll 1 \\ \dfrac{\ln(2B) - 0.577216 + \frac{4}{\pi B} - \frac{\ln(2B)}{2B^2}}{1 + \frac{8}{3\pi B}} & \text{for } B > 2.5 \end{cases} \tag{2}$$

depending on the dimensionless group:

$$B = \eta_s/\eta a \tag{3}$$

In a previous paper we have shown for a octadecanoate monolayer with no protein that using this description leads to good agreement between experiment and theory. Effects like the viscosity of the LC domain, the deformation of the initially circular domain, and the presence of neighboring domains could be neglected. These findings are supported by experiments on the Brownian motion of individual domains[30] as well as by flow experiments in narrow channels.[31] There it has been shown that the electrostatic dipole interaction responsible for the domain formation is too weak to have any effect on the rheological properties. However, our measurements and those performed in refs 30 and 31 contradict results obtained on two-dimensional colloidal suspensions[32] using a magnetic needle surface rheometer.[33−36] In colloidal suspension of three-dimensional charged colloids at interfaces the dipolar electrostatics has been found strong enough to have an effect on the rheology.[37] In some of our experiments the rotating domain will collide with another domain while being trapped. We discarded the motion of the domain while it collided and did not use it for data evaluation. Here we extend the optical tweezers experiments to situations, where the Boussinesq number B falls into the range

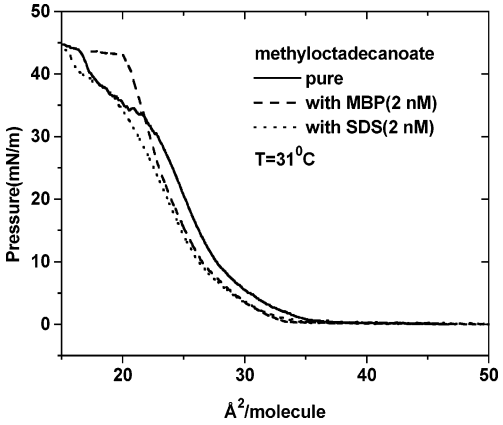

Figure 3. Surface pressure vs area isotherms of a methyl octadecanoate monolayer at $T = 31$ °C without and with MBP (SDS) adsorbed to the monolayer.

$0 < B < 50$. We fit the value of f_R/f_T in eq 1 to the alignment kinetics of our experimental domains and then numerically invert eq 2 to obtain B. The radius a of the rotating domain is measured, and the viscosity of water is $\eta(T = 35\ °C) = 0.7$ mPa s. Using eq 3, we then obtain the surface shear viscosity η_s. The method for measuring surface viscosities presented here is new and extends the sensitivity of older techniques toward lower viscosities. Note that the force of the tweezer exceeds the hydrodynamic drag at all times such that one does not need to calibrate the force of the tweezers. It is not used in the analysis. It would be useful to compare the technique with other techniques. A particle tracking technique introduced by Sickert and Rondelez[38] claims similar sensitivity. However, so far only a mathematical description neglecting Marangoni effects[39] exists for spheres protruding into the subphase, which when being used makes the rheological data not reliable at low viscosities as explained in refs 40 and 41.

Results

Despite many papers and books, which state the role of MBP for compactification of myelin sheets thus serving as a "glue" for lipids, it is still unclear how the protein−lipid interaction is maintained. Therefore, it is important to investigate the structural, adhesive, and dynamic properties of MBP. The present study aims at a quantitative measure of the compaction power 18.5 kDa MBP exhibits on monolayers that mimic the cytoplasmic leaflet of the myelin membrane. Therefore, we measure the surface shear viscosity of a Langmuir monolayer (methyl octadecanoate) upon adsorption of MBP from an aqueous subphase.

Pressure vs area isotherms at $T = 31$ °C of pure methyl octadecanoate and of methyl octadecanoate with MBP (SDS) absorbed from a 2 nM aqueous MBP (SDS) subphase are displayed in Figure 3. They give an estimate of the change in phase behavior due to the adsorption of MBP. In the phase coexistence region of the liquid condensed (LC) and liquid expanded (LE) phase at an area per molecule of ≈45 Å^2 per molecule, where we performed the rheological experiments, the surface pressure is below the resolution of our Wilhelmy system, such that no effect of the MBP is visible. However, at higher surface coverage, the surface pressure of the monolayer with MBP might differ significantly from the bare monolayer, and the phase transition densities are shifted by as much as 5 Å^2 per molecule.

Because of the Stokes paradox, the translational mobility of objects moving on the air/water surface within a monolayer is less sensitive to the rheological properties of the monolayer than the rotational mobility. Comparing the rotational motion of a liquid condensed domain in a monolayer with the translational motion (Figure 2) therefore sensitively reveals the surface shear viscosity η_s of a monolayer.

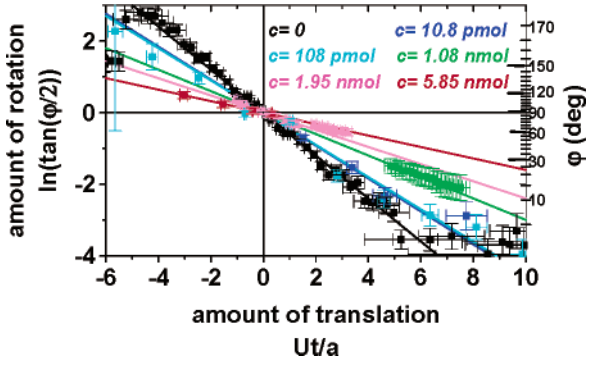

Figure 4. Plot of the amount of rotation (ln(tan(φ/2)) left axis, φ right axis) of the trapped domain as a function of the amount of translation (dimensionless time Ut/a) of noncaptured domains at various subphase concentrations of myelin basic protein. It is easier to rotate at low myelin basic protein concentration. At higher myelin basic protein concentration the surface shear viscosity increases and rotating the domains gets comparably more difficult than translating the domains.

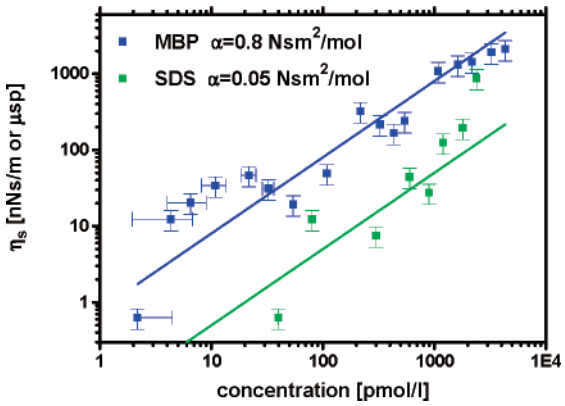

Figure 5. Surface shear viscosity of the liquid expanded phase of methyl octadecanoate upon adsorption of MBP or SDS, as extracted from the flow alignment experiments, showing a linear increase as a function of the MBP (SDS) subphase concentration.

Figure 4 shows plots of ln(tan(φ/2) and φ (left and right axis, respectively) versus the dimensionless time Ut/a of a methyl octadecanoate monolayer, with different concentrations of MBP dissolved into the aqueous subphase and fitted according to eq 1. We have used eq 2 and the viscosity of water $\eta(T = 35\ °C) = 0.7$ mPa s to convert the fitted value f_R/f_T into a surface shear viscosity η_s. In Figure 5 we plot the surface shear viscosity of the liquid monolayer phase as a function of the concentration c of MBP dissolved in the aqueous subphase of depth $d = 3$ mm, revealing a linear increase of the surface shear viscosity $\eta_s = \alpha c$ ($\alpha = 0.8$ N s m^2/mol) with the subphase concentration. Note that the concentrations of MBP used are very low. Assuming that all MBP adsorbs to the monolayer, one estimates an average separation of the proteins larger than 100 nm at all used concentrations. The conformation of MBP in aqueous solution is a random coil with a radius of gyration of the order of 5 nm. Without conformational change upon adsorption, there is no way in explaining how such tiny amount of protein could possibly have any effect on the surface rheological properties.

In 3d systems below the overlap concentration c^*, entanglement does not play a role. The viscosity of a d-dimensional dilute solution of polymers when neglecting hydrodynamic

interactions between the polymers can be described by Einstein's relation $\eta_{eff} = \eta[1 + [(d + 2)/(d - 1)]\phi]$, where η is the solvent viscosity, d the dimension of the liquid, and ϕ the volume fraction of polymer. Einstein's relation is based on the polymer solute being significantly more viscous than the solvent. The effective viscosity of the complex monolayer in the nonentangled regime is therefore linear in the concentration. Above the overlap concentration c^*, the effective viscosity rises much steeper than linear with the concentration as the number of entanglements gets larger and larger. This should be even more pronounced in a two-dimensional system. If the MBPs were entangled, the viscosity should rise with a stronger power than observed for polymers in 3d. Below the overlap concentration, a linear relation between viscosity and concentration is expected. However, as hydrodynamic interactions are of much longer range in 2d than in 3d, one expects the coefficient $(d + 2)/(d - 1)$ in Einstein's relation in 2d to be substantially renormalized by the hydrodynamic interactions. Indeed, the unrenormalized Einstein relation predicts a maximum increase of the viscosity of a factor of 5 as one increases the area fraction from zero to one. In the experiment an increase of viscosity of 4 orders of magnitude is observed. The measurements therefore suggest that the single protein unfolds at the surface to an extent which allows for significant hydrodynamic interaction, but presumably entanglements with the neighboring proteins at the surface are still negligible. Also, the arrangement of MBP at the monolayer surface might not be entirely statistical. An arrangement of the MBP in form of a 2d network could also explain part of the viscosity increase. Unfolding of the protein at bilayer membranes has been reported previously[7,8] using different techniques. This work shows that there is an intimate relation between structural properties of the protein, such as secondary and tertiary folding. It can be unraveled when working at concentrations below the 2d overlap concentration of MBP, where entanglements between the proteins at the surface are negligible and do not yet affect the dynamic properties such as the surface rheological properties of the membraneous lipid environment.

That entanglements indeed are negligible can be shown by measuring the effect of sodium dodecyl sulfate (SDS)—a simple anionic highly viscous[42] soluble surfactant—on the surface rheological behavior. Here entanglements are impossible. The same linear increase with the SDS subphase concentration is observed at higher molarities than with MBP.

For solid particles or highly viscous 2d droplets immersed into a monolayer, the effective viscosity of the suspension will depend on both the area fraction Φ of suspended particles and the hydrodynamic radius r of the individual suspended particle $\alpha = \alpha(\Phi, \eta_s/\eta r)$. At the same area fraction smaller particles lead to higher effective viscosities than larger particles because a larger fraction of hydrodynamic interaction is mediated via the 2d monolayer, while larger particles mediate the hydrodynamic interaction more via the subphase. It is therefore not straightforward to deduce the hydrodynamic radius r_{MBP} of MBP by comparing the prefactor α_{MBP} measured in Figure 5 for MBP with the value for SDS. However, from the above consideration it is clear that the hydrodynamic radius r_{MBP} of MBP in the monolayer must be larger than $r_{MBP} > \alpha_{MBP}/\alpha_{SDS} r_{SDS}$. Using $r_{SDS} \approx 0.5$ nm,[43] one estimates $r_{MBP} > 8$ nm, which is supported by measurements of Haas et al.[14] Hence, the viscosity increase due to the adsorption of MBP at the monolayer suggests that there indeed is a conformational change, and most of the amino acids forming the MBP indeed are in close contact with the monolayer interface.

It would therefore be interesting to access the frequency dependence of the viscosity in the nano−pico molar subphase concentration regime to verify this hypothesis. However, frequency-dependent rheology to this end is sensitive to surface viscosities in the msp range. The data displayed in Figure 5 show that the viscosities below the overlap concentration are significantly smaller than that.

Conclusions

Rheological measurements of a monolayer upon adsorption of myelin basic protein reveal an increase of 4 orders in magnitude of the surface shear viscosity with the concentration of myelin basic protein in the subphase. The increase is a result of a conformational change of the protein when adsorbing at the monolayer, increased hydrodynamic interactions that are more long range in a quasi-2-dimensional system than in 3 dimensions or due to a nonuniform distribution of the protein at the monolayer surface.

Appendix

The calculation of the viscous drag onto a solid disk moving in a monolayer underlying a deep subphase has been outlined analytically in the limit of large Boussinesq number and vanishing Boussinesq number.[24] Here we complete this work by deriving the asymptotic behavior for low Boussinesq numbers and performing a first-order expansion in the Boussinesq number of the dimensionless translational and rotational friction coefficients (eq 2a). Consider a 2d solid circular droplet (radius a) moving in a monolayer surroundings of surface shear viscosity η_s on top of an infinitely extended subphase of viscosity η. The flow of the subphase is described by the Stokes equations and the continuity equation

$$-\nabla p + \eta \nabla^2 \mathbf{u} = 0 \quad \text{and} \quad \nabla \cdot \mathbf{u} = 0 \tag{A1}$$

where p is the subphase pressure and $\mathbf{u}$ denotes the subphase velocity. The dynamic stress tensor is given by

$$\sigma = -p + \frac{\eta}{2}(\nabla \mathbf{u} + (\nabla \mathbf{u})^t) \tag{A2}$$

The general solution of (A1) in a cylindrical coordinate system (r,ϑ,z) can be written as[44]

$$\mathbf{u} = \nabla \Xi + \nabla \times (\mathbf{e}_z \Psi) + r \frac{\partial}{\partial r}(\nabla \Pi) + \mathbf{e}_z \frac{\partial \Pi}{\partial z} \quad \text{and}$$

$$p = -2\eta \frac{\partial^2 \Pi}{\partial z^2} \tag{A3}$$

where Ξ, Ψ, and Π are scalar functions solving the Laplace equation

$$\nabla^2 \{\Xi, \Psi, \Pi\} = \{0,0,0\} \tag{A4}$$

From the velocity boundary conditions $u_z(z = 0) = 0$ and from the incompressibility of all monolayer phases $\nabla_s \cdot \mathbf{u}_s = 0$ (∇_s and $\mathbf{u}_s$ are the surface gradient and the surface velocity) it follows that $\Pi = \Xi = 0$, and all streamlines are lying in planes parallel to the air/water interface. The remaining stream function Ψ which is in accordance with the symmetry of the problem is

$$\Psi_T(r,\vartheta,z) = 2Ua \sin\vartheta \int_0^\infty \mathrm{d}s\, s^{-1} b_T(s)\, J_1\left(s \frac{r}{R}\right) \mathrm{e}^{-(z/R)s}$$

$$\Psi_R(r,\vartheta,z) = \omega a^2 \int_0^\infty \mathrm{d}s\, s^{-1} b_R(s)\, J_0\left(s \frac{r}{R}\right) \mathrm{e}^{-(z/R)s} \tag{A5}$$

for the translational and rotational problem where U has the dimension of a velocity and ω of a angular frequency $b(s)$ is a dimensionless function of s to be determined; $J_n(sr/a)$ is the Bessel function of order n and argument sr/a. At the disk surface it is required that

$$\mathbf{u}_T = U\mathbf{e}_x$$
$$\mathbf{u}_R = \omega a\mathbf{e}_\vartheta \tag{A6}$$

The fluid motion of the liquid expanded phase obey the 2d Stokes equation:

$$-\nabla_s\pi_m + \eta\left(\frac{\partial \mathbf{u}}{\partial z}\right)_s + \eta_s\Delta_s\mathbf{u}_{sr} = 0 \tag{A7}$$

Here π_m is the surface pressure of the monolayer, ∇_s is the surface gradient, the second term is the viscous drag force from the subphase, and the third term is the viscous stress from the monolayer. The surface dynamic stress tensor is given by

$$\sigma_s = -\pi_m + \frac{\eta_s}{2}(\nabla_s\mathbf{u}_s + (\nabla_s\mathbf{u}_s)^t) \tag{A8}$$

The expression

$$B = \eta_s/\eta a \tag{A9}$$

defines a dimensionless group. Expansion around $B = 0$ leads to the solutions

$$b_T(s) = \sqrt{\frac{2}{\pi}}\left[\frac{J_{1/2}(s)}{s^{1/2}}(1 - sB) + \frac{B}{\pi}\sum_m(-1)^m\frac{2m + {}^3/_2}{(m+1)(m+{}^1/_2)}\frac{J_{2m+3/2}(s)}{s^{1/2}}\right] + O(B^2)$$

$$b_R(s) = \sqrt{\frac{8}{\pi}}\left[\frac{J_{3/2}(s)}{s^{1/2}}(1 - sB) + \frac{B}{\pi}\sum_m(-1)^m\frac{4m+1}{(m+1)({}^1/_2 - m)}\frac{J_{2m+1/2}(s)}{s^{-1/2}}\right] + O(B^2) \tag{A10}$$

The drag force is a sum of the force from the area at the disk and the edge

$$F_{\text{sub}} = \int_A \sigma\cdot\mathbf{n}\,\mathrm{d}A = -2\pi aU\eta\int_0^\infty \mathrm{d}s\; b_T(s)\,J_1(s) \tag{A11a}$$

$$F_{\text{edge}} = \int_P \sigma_s\cdot\mathbf{n}\,\mathrm{d}s = -2\pi aU\eta\int_0^\infty \mathrm{d}s\; b_T(s)\,J_1(s) \tag{11b}$$

and

$$F_{\text{drag}} = F_{\text{sub}} + F_{\text{edge}} = 8\eta Ua(1 + B) + O(B^2) = f_T\eta Ua \tag{A12}$$

Similarly we find for the torque

$$\tau_{\text{sub}} = \int_A \mathbf{r}\times\sigma\cdot\mathbf{n}\,\mathrm{d}A = -2\pi a^3\omega\eta\int_0^\infty \mathrm{d}s\; b_R(s)\,J_2(s) \tag{A13a}$$

$$\tau_{\text{edge}} = \int_P \mathbf{r}\times\sigma_s\cdot\mathbf{n}\,\mathrm{d}s = -2\pi a^3\omega\eta\int_0^\infty \mathrm{d}s\; b_R(s)\,BsJ_2(s) \tag{A13b}$$

such that the total torque equals

$$\tau_{\text{R}} = \tau_{\text{sub}} + \tau_{\text{edge}} = \frac{16}{3}\left(1 + \frac{6}{\pi}B\right)\omega\eta a^3 := f_R\omega\eta a^3 \tag{A14}$$

with the definitions (A12) and (A14) for the dimensionless friction coefficients f_T and f_R one finds

$$\frac{f_R}{f_T} = \frac{2}{3}\left(1 + \left[\frac{6}{\pi} - 1\right]B\right) + O(B^2) \tag{A15}$$

References and Notes

(1) Huxley, A. F.; Stampell, R. Evidence for saltatory conduction in peripheral myelinated nerve fibers. *J. Physiol.* **1949**, *108*, 315.

(2) Lemke, G. Unwrapping the genes of myelin. *Neuron* **1988**, *1*, 535.

(3) Campagnoni, A. T. Molecular biology of myelin proteins from the central nervous system. *J. Neurochem.* **1988**, *51*, 1.

(4) Smith, R. The basic protein of CNS myelin: its structure and ligand binding. *J. Neurochem.* **1992**, *59*, 1589.

(5) Krigbaum, W. R.; Hsu, T. S. Molecular conformation of bovine A1 basic protein, a coiling macromolecule in aqueous solution. *Biochemistry* **1975**, *14*, 2542.

(6) Mendz, G. L.; Moore, W. J.; Martenson, R. E. Interaction of myelin basic protein with micelles of dodecylphosphocholine *Biochemistry* **1984**, *23*, 6041.

(7) Keniry, M. A.; Smith, R. Circular dichroic analysis of the secondary structure of myelin basic protein and derived peptides bound to detergents and lipid vesicles. *Biochim. Biophys. Acta* **1979**, *578*, 381.

(8) Keniry, M. A.; Smith, R. Dependence on lipid structure of coil-to-helix transition of bovine myelin basic protein. *Biochim. Biophys. Acta* **1981**, *668*, 107.

(9) Mendz, G. L.; Brown, L. R.; Martenson, R. E. Interactions of myelin basic protein with mixed dodecylphosphocholine/palmitoyllysophosphatidic acid micelles. *Biochemistry* **1990**, *29*, 2304.

(10) Boggs, J. M.; Moscarello, M. A.; Papahadopoulos, D. In *Lipid−Protein Interactions*; Jost, P., Griffith, O. H., Eds.; John Wiley and Sons: New York, 1982; Vol. 2, pp 1−51.

(11) Beniac, D. R.; Luckevich, M. D.; Czarnota, G. J.; Tompkins, T. A.; Ridsdale, R. A.; Ottensmeyer, F. P.; Moscarello, M. A.; Harauz, G. Three-dimensional structure of myelin basic protein 0.1. Reconstruction via angular reconstitution of randomly oriented single particles. *J. Biol. Chem.* **1997**, *272*, 4261.

(12) Ridsdale, R. A.; Beniac, D. R.; Tompkins, T. A.; Moscarello, M. A.; Harauz, G. Three-dimensional structure of myelin basic protein 0.2. Molecular modeling and considerations of predicted structures in multiple sclerosis. *J. Biol. Chem.* **1997**, *272*, 4269.

(13) Haas, H.; Torrielli, M.; Steitz, R.; Cavatorta, P.; Sorbi, R.; Fasano, A.; Riccio, P.; Gliozzi, A. Myelin model membranes on solid substrates. *Thin Solid Films* **1998**, *327*, 627.

(14) Haas, H.; Oliveira, C. L. P.; Torriani, I. L.; Polverini, E.; Fasano, A.; Carlone, G.; Cavatorta, P.; Riccio P. Small-angle X-ray scattering from lipid-bound myelin basic protein in solution. *Biophys. J.* **2004**, *86*, 455.

(15) Polverini, E.; Fasano, A.; Zito, F.; Riccio, P.; Cavatorta, P. Conformation of bovine myelin basic protein purified with bound lipids. *Eur. Biophys. J. Biophys. Lett.* **1999**, *28*, 351.

(16) Bates, I. R.; Feix, J. B.; Boggs, J. M.; Harauz, G. An Immunodominant Epitope of Myelin Basic Protein Is an Amphipathic α-Helix. *J. Biol. Chem.* **2004**, *279*, 5757.

(17) Readhead, C.; Popko, B.; Takahashi, N.; Shine, S. H.; Saavedra, R. A.; Sidman, P. L.; Hood, L. Expression of a myelin basic protein genen in transgenic mice: correction of the dismyelination phenotype. *Cell* **1987**, *48*, 703−712.

(18) Swaminathan, R.; Bicknese, S.; Periasamy, N.; et al. *Biophys. J.* **1996**, *71*, 1140.

(19) Karolin, J.; Johansson, L. B. A.; Strandberg, L.; Ny, T. *J. Am. Chem. Soc.* **1994**, *116*, 7801.

(20) Redfield, C.; Boyd, J.; Smith, L. J.; Smith, R. A. G.; Dobson, C. M. *Biochemistry* **1992**, *31*, 10431.

(21) Mackay, J. P.; Shaw, G. L.; King, G. F. *Biochemistry* **1996**, *35*, 4867.

(22) Pralle, A.; Prummer, M.; Florin, E. L.; Stelzer, E. H. K.; Horber, J. K. H. *Microsc. Res. Tech.* **1999**, *44*, 378.

(23) Saffman, P. G.; Delbrück, M. *Proc. Natl. Acad. Sci. U.S.A.* **1975**, *72*, 3111.

(24) Hughes, B. D.; Pailthorpe, B. A.; White, L. R. *J. Fluid Mech.* **1981**, *110*, 349.

(25) Pralle, A.; Keller, P.; Florin, E. L.; Simons, K.; Horber, J. K. H. *J. Cell Biol.* **2000**, *148*, 997.

(26) Steffen, P.; Heinig, P.; Wurlitzer, S.; Khattari, Z.; Fischer, T. M. The translational and rotational drag on Langmuir monolayer domains. *J. Chem. Phys.* **2001**, *115*, 994.
(27) Nassoy, P. Birch, W. R.; Andelman, D.; Rondelez, F. *Phys. Rev. Lett.* **1996**, *76*, 455.
(28) Wurlitzer, S.; Steffen, P.; Wurlitzer, M.; Khattari, Z.; Fischer, T. M. *J. Chem. Phys.* **2000**, *113*, 3822.
(29) Equation 1 implies that the clock measuring the time is set to zero, when the lever arm ecncloses an angle of $\varphi = \pi/2$ with the flow direction.
(30) Klingler, J. F.; McConnell, H. *J. Phys. Chem.* **1993**, *97*, 6096.
(31) Schwartz, D.; Knobler, C. M.; Bruinsma, R. *Phys. Rev. Lett.* **1994**, *73*, 2841.
(32) Ding, J. Q.; Warriner, H. E.; Zasadzinski, J. A. *Phys. Rev. Lett.* **2002**, *88*, 168102.
(33) Brooks, C. F.; Fuller, G. G.; Frank, C. W.; Robertson, C. R. *Langmuir* **1999**, *15*, 2450.
(34) Fischer, T. M. *J. Fluid Mech.* **2004**, *498*, 123.
(35) Levine, A. J.; Liverpool, T. B.; MacKintosh, F. C. *Phys. Rev. E* **2004**, *69*, 021503.
(36) Alonso, C.; Zasadzinski, J. A. *Phys. Rev. E* **2004**, *69*, 021602.
(37) Stancik, E. J.; Gavranovic, G. T.; Wildenbrant, M. J. O.; Laschitsch, A. T.; Vermant, J.; Fuller, G. G. *Faraday Discuss.* **2003**, *123*, 145.
(38) Sickert, M.; Rondelez, F. *Phys. Rev. Lett.* **2003**, *90*, 126104.
(39) Danov, K.; Aust, R.; Durst, F.; Lange, U. *J. Colloid Interface Sci.* **1995**, *175*, 36.
(40) Fischer, T. M. *Phys. Rev. Lett.* **2004**, *92*, 139603.
(41) Sickert, M.; Rondelez, F. *Phys. Rev. Lett.* **2004**, *92*, 139604.
(42) The surface shear viscosity of an SDS monolayer above the critical micelle concentration cmc = 8.3 mM is $\eta_s = 2.6$ μN s/m. Cf.: Barentin, C.; Ybert, C.; DiMeglio, J. M.; Joanny, J. F. *J. Fluid Mech.* **1999**, *397*, 331−349. The SDS cosurfactant concentration in our experiments is at least 3 orders of magnitude lower than the cmc and the approximation of the SDS molecules as *solid* inclusions into the methyl octadecanoate monolayer is an adequate approximation.
(43) Here we treat the SDS molecule as a solid object immersed into an otherwise homogeneous fluid. In reality, the Stokes equation, a continuum approximation for the octadecanoate surfactant molecules, will no longer hold on the molecular scale. Nevertheless, the same approximation has been proven to be useful for the treatment of proteins in membranes (cf. ref 23) which have hydrodynamic radii 1 order of magnitude larger than SDS. Treating the SDS molecule in the same way stretches the theory to its limits. However, we believe it to be still useful for an order of magnitude estimate.
(44) Happel, J.; Brenner, H. *Low Reynolds Number Hydrodynamics;* Martinus Nijhoff Publishers: The Hague, 1983; p 77.